Front. Earth Sci. 2018, 12(1): 95–107
https://doi.org/10.1007/s11707-016-0620-1

RESEARCH ARTICLE

Impact of water depth on the distribution of iGDGTs in the surface sediments from the northern South China Sea: applicability of TEX_{86} in marginal seas

Jiali CHEN[1,2,5], Pengju HU[1,2], Xing LI[1,3], Yang YANG[1], Jinming SONG[4], Xuegang LI[4], Huamao YUAN[4], Ning LI[4], Xiaoxia LÜ (✉)[1,3]

1 State Key Laboratory of Biogeology and Environmental Geology, China University of Geosciences, Wuhan 430074, China
2 Faculty of Earth Sciences, China University of Geosciences, Wuhan 430074, China
3 College of Marine Science and Technology, China University of Geosciences, Wuhan 430074, China
4 Institute of Oceanology, Chinese Academy of Sciences, Qingdao 266071, China
5 No.5 Middle School of Nan Chang, Nanchang 330029, China

Abstract The TEX_{86}^{H} paleothermometer on the base of isoprenoid glycerol dialkyl glycerol tetraethers (iGDGTs) has been widely applied to various marine settings to reconstruct past sea surface temperatures (SSTs). However, it remains uncertain how well this proxy reconstructs SSTs in marginal seas. In this study, we analyze the environmental factors governing distribution of iGDGTs in surface sediments to assess the applicability of TEX_{86}^{H} paleothermometer in the South China Sea (SCS). Individual iGDGT concentrations increase gradually eastwards. Redundancy analysis based on the relative abundance of an individual iGDGT compound and environmental parameters suggests that water depth is the most influential factor to the distribution of iGDGTs, because thaumarchaeota communities are water-depth dependent. Interestingly, the SST difference (ΔT) between TEX_{86}^{H} derived temperature and remote-sensing SST is less than 1°C in sediments with water depth > 200 m, indicating that TEX_{86}^{H} was the robust proxy to trace the paleo-SST in the region if water depth is greater than 200 m.

Keywords iGDGTs, distribution, South China Sea (SCS), sea surface temperature, water depth

1 Introduction

Phylogenomic analysis showed that Crenarchaeota and Euryarchaeota are two kingdoms, Crenarchaeota (Group I) and Euryarchaeota (Group II), within the domain of the Archaea. Recently, the Group I Archaea and their close relatives from terrestrial environments were reclassified as a separate phylum. Thaumarchaeota are likely the most ancient Archaea. Many studies confirm that Thaumarchaeota are among the most abundant organisms in the ocean, approximately 40% of all cells in the bathypelagic (e.g., Karner et al., 2001), whereas the Group II Euryarchaeota, in general, are less abundant and shown near the surface ocean (Pernthaler et al., 2002; Herndl et al., 2005).

Glycerol dialkyl glycerol tetraethers (GDGTs) are characteristic membrane lipids of Archaea and bacteria. GDGTs have been reported in almost every type of environment, such as soils (e.g., Weijers et al., 2007; Yang et al., 2014), lacustrine water columns and sediments (e.g., Powers et al., 2010; Weber et al., 2015), and marine water columns and sediments (e.g., Schouten et al., 2002; Basse et al., 2014). GDGTs include mainly two types: isoprenoidal GDGTs (iGDGTs) and branched GDGTs (bGDGTs) (Fig. 1). Isoprenoidal GDGTs are produced from two groups of Archaea: Thaumarchaeota (formerly marine group I Crenarchaeota) and Euryarchaeota. Cyclopentane moieties increase with growth temperature (De Rosa et al., 1980; Gliozzi et al., 1983). The TEX_{86} (TetraEther index of tetraethers consisting of 86 carbon atoms) was thus constructed to trace the paleo-sea surface temperature, SST (Schouten et al., 2002), which has been recalibrated to improve the accuracy of reconstructing the paleo-SSTs in different environments (e.g., Sluijs et al., 2006; Kim et al., 2008; Liu et al., 2009; Kim et al., 2010). Kim et al. (2010) concluded that the TEX_{86}^{H} and TEX_{86}^{L} are the most promising proxies.

Branched glycerol dibiphytanyl glycerol tetraethers

Received March 2, 2016; accepted September 18, 2016

E-mail: luxiaox@163.com

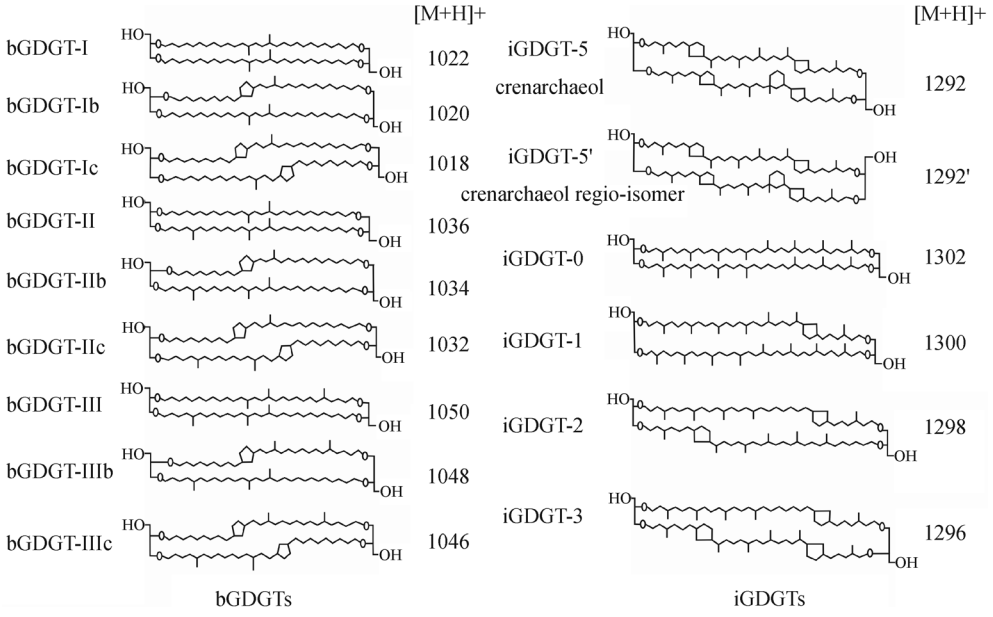

Fig. 1 Structures of branched GDGTs and isoprenoid GDGTs.

(bGDGTs) were reported to be produced mainly from the terrestrial bacteria in soil or peat environments although some *in situ* bGDGTs may exist in marine and lacustrine environments (Peterse et al., 2009; Sinninghe Damsté et al., 2009; Lü et al., 2014; Zell et al., 2015). Hopmans et al. (2004) proposed a BIT index (Branched Isoprenoid Tetraether Index) that can be used to estimate the relative contribution of terrestrial and aquatic organic matter to marine sediments (i.e., soil- and/or river-derived organic matter input). BIT value > 0.8 likely corresponds to a strong soil OM footprint while BIT value < 0.2 may be for a relatively low soil OM input (Walsh et al., 2008; Zhang et al., 2012).

The South China Sea (SCS) is the largest marginal sea in Southeast Asia with annual SST varying from 25°C to 29°C. Its climatic variations in the atmosphere and in the upper ocean are primarily dominated by the East Asian monsoon (Liu et al., 2002). The significant correlation between the sea surface temperature anomaly in summer and the equatorial sea surface temperature anomalies in the preceding winter suggest that the sea surface temperature anomaly could be considered as an indicator for the monsoon variations and El Niño and southern oscillation (ENSO) (Ose et al., 1997). Therefore, accurate SST reconstruction appears to be critical to study the inter-feedback between climate change and oceanic physical and chemical parameters. Study on SST reconstruction with GDGTs was conducted in the SCS during the last several years and results show that the TEX_{86}-derived temperature, used to trace the subsurface temperature or winter SST, was lower than the remote-sensing SST (Wei et al., 2011; Jia et al., 2012; Zhou et al., 2014). However, Shintani et al. (2011) argued that the TEX_{86}-derived temperature corresponded to the warm season temperature in the open northern SCS. The different findings by those researchers may be due to complex sources of sediments and insufficient knowledge about Thaumarchaeota. Up to date application of TEX_{86} to marginal seas is still limited, likely due to that (i) terrestrial input makes sources of GDGTs complicated, and (ii) spatial variability of environmental factors (such as nutrient concentrations, salinity, pH, and water depth) is significant.

In this study, we analyzed the iGDGTs in the surface sediments from the coastal northern SCS, and performed the redundancy analysis (RDA) to distinguish the controlling factors that influence spatial distribution of iGDGTs and further assessed the applicability of TEX_{86}^{H} as a temperature proxy in this region.

2 Material and methods

2.1 Study area and sampling sites

The South China Sea is the largest marginal sea in Southeast Asia, which connects to the Pacific Ocean through the Luzon Strait. The East Asian monsoon plays an important role in the SCS currents and the water temperature (Shen and Lau, 1995; Hu et al., 2000; Qu, 2001). In winter the SCS is dominated by the strong northeast monsoon, with an intense coastal current from northeast to southwest along the coast of Guangdong and the east coast of Hainan Island. The strong northeast monsoon transports cold water from the north and causes a distinctly lower water temperature. In summer, the wind becomes weak and reverses direction to southwest (Hu

et al., 2000).

A total of 28 surface sediments were collected from coastal to deep water (2−505 m) in the north SCS (Fig. 2) and then refrigerated at −20°C prior to being further analyzed.

2.2 Lipid analysis

After frozen and ground, about 15 g of sediments were extracted ultra-sonically with DCM/MeOH (9:1, v/v) for 15 min and were extracted at least 3 times. Supernatants from each extraction were collected and combined after centrifugation. The total lipid extracts (TLEs) were concentrated to 1−2 mL with a rotary evaporator and dried with N_2 in a 2 mL vial. The TLEs were separated into apolar-fraction (F1) and polar-fraction (F2) using an activated Al_2O_3 column eluted with hexane and MeOH, respectively. The F2 fraction was condensed to 1−2 mL with N_2 and filtered through a 0.45 μL PTFE filter. The filtered F2 fraction was dried with N_2 (Yang et al., 2014), then dissolved in 300 mL hexane/isopropanol (99:1, v/v), with a C_{46} glycerol trialkyl glycerol tetraether (C_{46}GTGT) added as internal standard (Huguet et al., 2006). GDGTs were analyzed using an Agilent 1200 series liquid chromatograph and 6460A triple quadrupole mass spectrometer equipped with an autosampler and ChemStation manager software. An aliquot of sample (10−30 μL) was injected and separation was achieved with an Alltech Prevail Cyano column (150 mm×2.1 mm, 3 μm; Grace, Deerfield, IL, USA). The elution gradient followed that of Schouten et al. (2007) with minor modifications. GDGTs were eluted isocratically in the first 5 min with A/B 9:1 (v/v), where A = hexane and B = hexane/isopropanol (9:1, v/v). The following linear gradient was then used: 90/10 A/B to 82/18 A/B from 5 to 45 min, followed by 100% B (10 min) to wash the column and then 90/10A/B to equilibrate it. GDGTs were detected using selected ion monitoring (SIM), targeting m/z 1302,1300, 1298, 1296, 1292, 1050, 1048, 1046, 1036, 1034, 1032, 1022, 1020, 1018, 653, and 744. Relative abundance was determined from the peak area integration of $[M + H]^+$ in the extracted ion chromatograms. Unless noted specifically, the fractional abundance of an individual GDGT compound is proportional to the total iGDGTs or bGDGTs (Yang et al., 2014). The final concentration should be considered semi-quantitative because we did not determine the response factors for GDGTs vs. the C_{46} GTGT standard.

2.3 Environmental parameters and statistical analysis

Environmental parameters for each sampling site were obtained from NOAA (http://www.esrl.noaa.gov/) and the Alfred Wegener Institute (http://odv.awi.de/en/data/ocean/). SST and mean annual temperatures at 20 m and 50 m for each sampling site were retrieved from NOAA (http://www.esrl.noaa.gov/psd/), and annual mean values of total alkalinity (TAlk) and NO_3^- were obtained from literature. 10-yr average values of the annual and seasonal SST and mean annual salinity SST data were used to explore the relationship of the iGDGT distributions with environmental parameters (Table 1) because longer times may be needed for suspended particles to settle down to the bottom. The sedimentation rates in the South China Sea are about 0.19−0.47 cm/yr (Li, 1988; Li and Yuan, 1991). Therefore, 10-yr average values were used to reduce such bias caused by ephemeral environmental parameters.

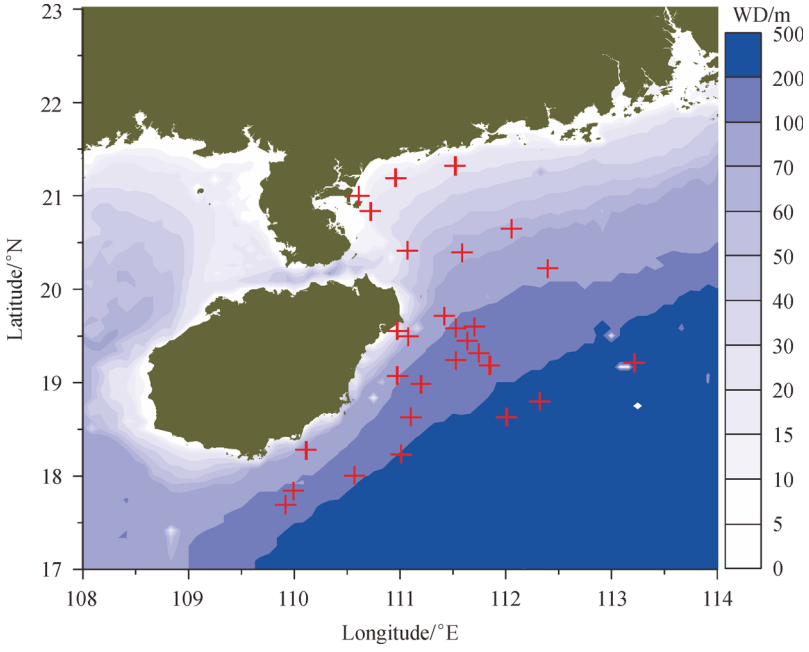

Fig. 2 Sampling sites in the SCS. WD: water depth.

Table 1 Environmental parameters (water depth is obtained *in situ* using CTD; other parameters are obtained from two online datasets)

Site	Longitude /(°E)	Latitude /(°N)	TEX_{86}^{H}	TEX_{86}^{H}-SST /°C	Water depth /m	Salinity /psu	NO_3^- /(μmol·L^{-1})	TALK /(μmol·kg^{-1})	Oxygen /(mL·L^{-1})	TCO_2 /(μmol·kg^{-1})	AM-SST /°C	SST-Spring /°C	SST-Summer /°C	SST-Autumn /°C	SST-Winter /°C
S-1	111.53	21.32	−0.28	19.48	18.30	33.65	0.62	2079.00	4.90	1911.50	25.22	23.89	29.15	27.19	20.62
S-2	112.06	20.65	−0.25	21.22	60.80	33.87	0.56	2091.00	4.86	1912.00	25.71	24.72	29.04	27.31	21.79
S-3	112.40	20.22	−0.22	23.43	80.00	33.93	0.55	1092.00	4.85	1912.00	26.04	25.24	29.03	27.45	22.47
S-4	113.22	19.21	−0.17	27.03	453.00	33.94	0.57	2089.00	4.80	1909.00	26.75	26.39	29.21	27.75	23.59
S-5	110.96	21.19	−0.29	18.55	12.70	33.56	0.59	2070.00	4.89	1910.50	25.12	23.77	29.29	27.22	20.48
S-6	111.59	20.39	−0.25	21.16	62.10	33.91	0.55	1091.00	4.85	1911.50	25.77	24.79	29.17	27.42	21.79
S-7	110.61	20.99	−0.28	19.53	2.70	33.50	0.56	2062.00	4.88	1909.00	25.21	23.77	29.31	27.26	20.50
S-8	110.73	20.83	−0.26	20.78	14.40	33.58	0.56	2069.00	4.87	1910.50	25.32	23.99	29.33	27.30	20.76
S-9	111.07	20.41	−0.29	18.78	40.60	33.79	0.55	2082.00	4.85	1911.00	25.69	24.59	29.26	27.39	21.49
S-10	111.70	19.59	−0.22	23.76	106.20	33.98	0.55	2091.00	4.81	1911.80	26.23	25.75	29.28	27.60	22.85
S-11	112.32	18.80	−0.17	27.04	330.00	33.96	0.59	2087.00	4.78	1908.50	26.83	26.62	29.26	27.78	23.73
S-12	111.42	19.71	−0.23	22.65	79.00	33.96	0.55	2090.00	4.81	1911.90	26.23	25.57	29.27	27.56	22.60
S-13	111.53	19.58	−0.23	22.65	100.70	33.98	0.55	2091.00	4.81	1911.80	26.33	25.75	29.27	27.60	22.81
S-14	111.64	19.45	−0.21	24.41	115.80	33.98	0.56	2091.00	4.80	1911.70	26.44	25.93	29.26	27.64	23.00
S-15	111.75	19.32	−0.20	25.00	132.70	33.98	0.56	2091.00	4.80	1911.50	26.53	26.07	29.26	27.68	23.14
S-16	111.85	19.18	−0.19	25.63	146.30	33.98	0.57	2090.00	4.80	1911.00	26.62	26.23	29.26	27.73	22.35
S-17	110.98	19.55	−0.22	23.58	20.70	33.85	0.54	2084.00	4.81	1911.00	26.26	25.59	29.34	27.61	22.62
S-18	111.08	19.49	−0.27	19.89	66.30	33.91	0.54	2086.00	4.80	1911.50	26.35	25.73	29.34	27.62	22.75
S-19	111.53	19.24	−0.20	24.66	124.90	33.98	0.56	2089.00	4.79	1910.80	26.56	26.12	29.32	27.72	23.23
S-20	110.98	19.07	−0.25	21.73	99.70	33.90	0.56	2084.00	4.79	1910.50	26.87	26.14	29.41	27.73	23.25
S-21	111.20	18.98	−0.23	22.89	120.60	33.94	0.57	2087.00	4.79	1910.30	26.93	26.16	29.40	27.73	23.42
S-22	112.01	18.63	−0.18	26.49	504.70	33.96	0.60	2086.00	4.75	1908.00	26.93	26.74	29.35	27.82	23.87
S-23	111.11	18.63	−0.21	24.43	147.80	33.93	0.58	2083.00	4.72	1909.00	26.92	26.62	29.44	27.82	23.75
S-24	111.02	18.23	−0.18	26.07	410.70	33.89	0.57	2081.00	4.76	1907.50	27.11	26.89	29.50	27.93	24.12
S-25	110.12	18.27	−0.23	22.91	42.70	33.75	0.49	2074.00	4.74	1908.00	26.95	26.59	29.53	27.83	23.89
S-26	110.57	18.01	−0.24	22.46	156.80	33.82	0.53	2077.00	4.74	1907.50	27.17	26.93	29.53	27.93	24.25
S-27	109.99	17.84	−0.23	22.94	66.00	33.74	0.49	2070.00	4.71	1907.20	27.13	26.81	29.56	27.93	24.24
S-28	109.92	17.69	−0.23	22.73	105.70	33.73	0.49	2068.00	4.71	1907.00	27.17	26.84	29.58	27.95	24.29

Relative abundance of each iGDGT component was obtained by normalizing the peak area to the summed area of all iGDGTs (Table 2). Redundancy analysis (RDA) was used to assess the correlation between iGDGTs distribution and environmental parameters. TEX_{86}^{H} and TEX_{86}^{H} -derived temperature (abbreviated as TEX_{86}^{H} -SST in Table 1) were calculated according to the following formula (Kim et al., 2010),

$$TEX_{86}^{H} = LOG\left(\frac{[iGDGT\text{-}2] + [iGDGT\text{-}3] + [Cren']}{[iGDGT\text{-}1] + [iGDGT\text{-}2] + [iGDGT\text{-}3] + [Cren']}\right), = LOG(TEX_{86}) \quad (1)$$

$$T = 68.4 \times TEX_{86}^{H} + 38.6 \quad (R^2 = 0.87,\ n = 255,\ p < 0.0001). \quad (2)$$

BIT index proposed by Hopmans et al. (2004) was estimated by the following equation

$$BIT = \frac{[I] + [II] + [III]}{[I] + [II] + [III] + [Cren]}. \quad (3)$$

3 Results

3.1 The distribution of GDGTs

Total concentration of the iGDGTs in the SCS sediments (15.03−534.18 ng/g) is much higher than that of the bGDGTs (2.34–128.62 ng/g). Among all iGDGT compounds, crenarchaeol has the highest concentration (9.72–344.18 ng/g), followed by the iGDGT-0 (2.80–110.04 ng/g). The iGDGTs with 1–3 rings and the

Table 2 Relative abundance of iGDGTs in SCS sediment (%)

Site	iGDGT-0	iGDGT-1	iGDGT-2	iGDGT-3	Cren.	Cren.iso
S-1	0.33	0.08	0.06	0.02	0.50	0.01
S-2	0.21	0.07	0.05	0.02	0.64	0.01
S-3	0.25	0.09	0.08	0.03	0.52	0.02
S-4	0.22	0.07	0.08	0.02	0.56	0.05
S-5	0.21	0.05	0.04	0.01	0.68	0.01
S-6	0.22	0.06	0.05	0.02	0.64	0.01
S-7	0.22	0.06	0.04	0.02	0.65	0.01
S-8	0.22	0.06	0.04	0.03	0.64	0.01
S-9	0.22	0.06	0.04	0.01	0.67	0.01
S-10	0.19	0.06	0.06	0.02	0.64	0.02
S-11	0.21	0.07	0.08	0.02	0.57	0.05
S-12	0.20	0.06	0.06	0.02	0.64	0.02
S-13	0.20	0.07	0.05	0.02	0.64	0.02
S-14	0.13	0.07	0.07	0.02	0.68	0.03
S-15	0.18	0.07	0.06	0.02	0.64	0.03
S-16	0.19	0.07	0.07	0.02	0.61	0.03
S-17	0.19	0.07	0.06	0.03	0.65	0.01
S-18	0.23	0.06	0.04	0.02	0.63	0.01
S-19	0.19	0.07	0.06	0.02	0.64	0.02
S-20	0.21	0.06	0.05	0.02	0.65	0.01
S-21	0.20	0.07	0.06	0.02	0.64	0.02
S-22	0.22	0.07	0.08	0.02	0.56	0.04
S-23	0.19	0.07	0.07	0.02	0.62	0.02
S-24	0.19	0.07	0.07	0.02	0.61	0.04
S-25	0.19	0.06	0.05	0.02	0.66	0.01
S-26	0.20	0.06	0.05	0.02	0.65	0.01
S-27	0.21	0.06	0.06	0.02	0.64	0.02
S-28	0.21	0.06	0.05	0.02	0.64	0.02

crenarchaeol regio-isomer have the lowest concentrations (Fig. 3). The pattern of lipid distribution in these samples is generally characterized with 65% crenarchaeol, 12% cyclic iGDGTs, and 23% iGDGT-0 (Table 2).

Spatial distribution of each individual iGDGT compound shows a similar tendency (Fig. 3). Concentration of each iGDGT compound is lower near the coast and increases offshore. Peak values of iGDGT-0 and iGDGT-5

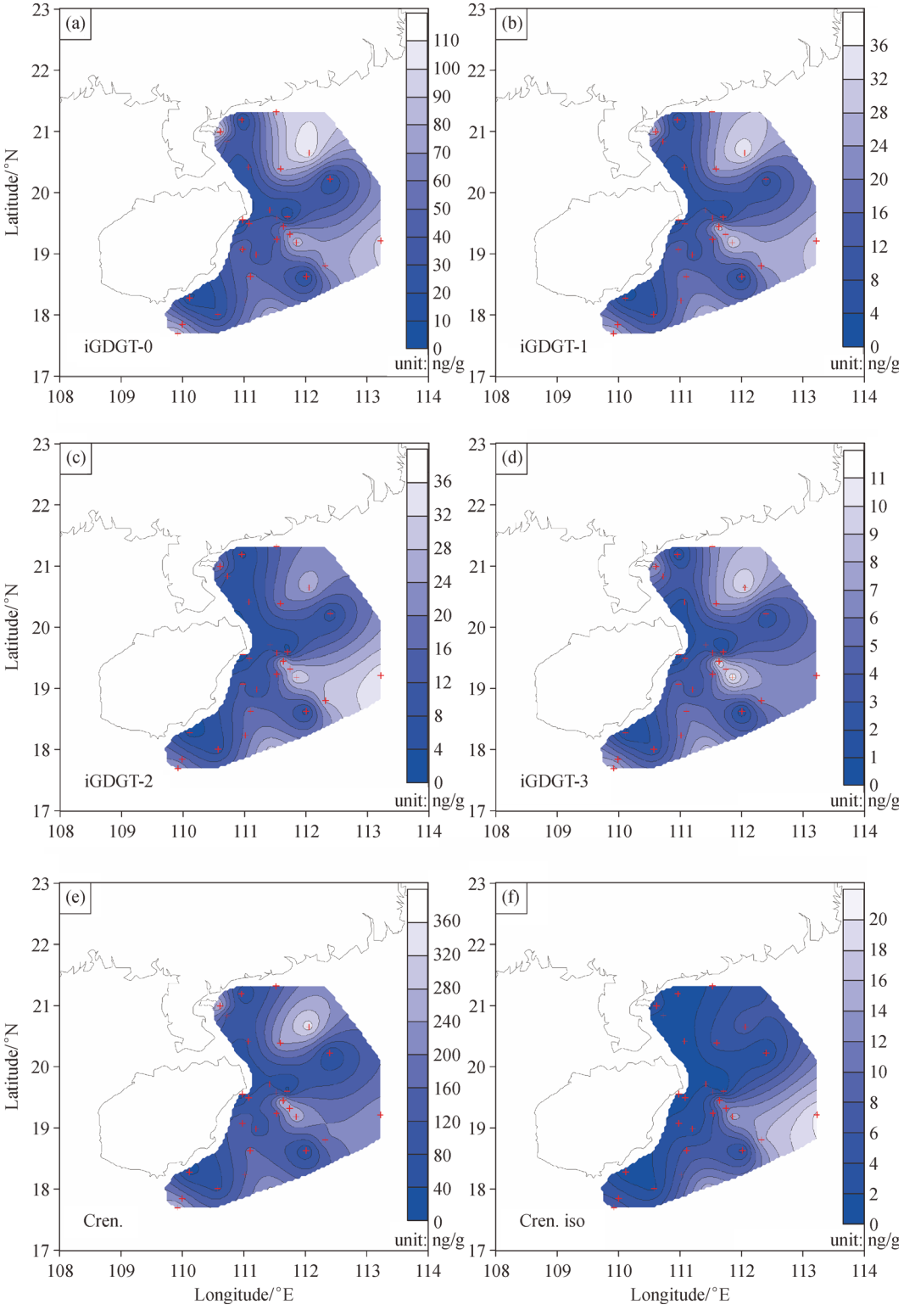

Fig. 3 The spatial distribution of iGDGTs concentration.

(Cren.) appear to be shown at the region centered at (112°E, 20.75°N) (Fig. 3). However, peak values of iGDGT-1–iGDGT-3 are shown at the region centered at (111.8°E, 19°N).

Concentration of the major bGDGTs (bGDGT-I + bGDGT-II + bGDGT-III) is higher than that of the total cyclic bGDGTs (bGDGT-Ib + bGDGT-Ic + bGDGT-IIb + bGDGT-IIc + bGDGT-IIIb + bGDGT-IIIc) (Lü et al., 2014). The distribution of bGDGTs is different from that of iGDGTs. Concentrations of the two types of bGDGTs decrease toward the offshore and the highest concentrations are shown at the northwest part of the study region (Fig. 4). The estimated BIT values are low, ranging from 0.02 to 0.26 at the study region (Fig. 5).

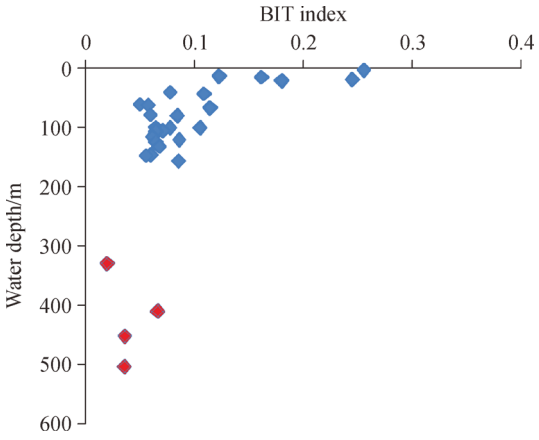

Fig. 5 The distribution of BIT.

3.2 Multivariate analysis

The redundancy analysis (RDA) show that the iGDGTs distribution is mostly influenced by nutrients, water depth, spring SST, and salinity ($p < 0.05$). The four environmental parameters contributed approximately 17%, 12%, 12%, and 9% to the variance, respectively (Fig. 6(a) and Table 3).

To distinguish the controlling factors to influence the TEX_{86}^{H} proxy, we further performed RDA using four iGDGT compounds for the TEX_{86}^{H} calculation (Fig. 6(b)). Water depth and nitrate explain 52% and 8% of the variance, respectively. Salinity and spring-SST show an insignificant influence on it (Fig. 6(b) and Table 4).

Correlation between the fractional abundance of individual iGDGTs and water depth was analyzed. The fractional abundance of the Crenarchaeol regio-isomer and iGDGT-2/iGDGT-3 ratio has a significant correlation with water depth, showing a strong increasing trend with water depth (Fig. 7).

3.3 SST derived from core-top sediments

The performance of the TEX_{86} calibration function could be evaluated from the residuals between the remote sensing SST and TEX_{86}-derived SST (Fig. 8). The residuals for TEX_{86}^{H} (Eq. (1)) ranged from – 2°C to 2.8°C in the global calibrations. The differences (ΔT) between TEX_{86}^{H} derived temperature and remote-sensing temperature at depth of 0 m, 20 m, and 50 m are shown in Fig. 8. The ΔT shows a decreasing trend with depth. Moreover, the ΔT between TEX_{86}^{H} derived temperature and remote-sensing temperature from 0–20 m is smaller than 1°C in the sediments with water depth > 200 m (Fig. 8). The TEX_{86}^{H} derived temperature in the shallow water sediment (< 200 m) is closer to the remote-sensing temperature at the depth of 50 m; ΔT (50 m) < ΔT (20 m) < ΔT (0 m). An inverse trend appears in the deep water sediment

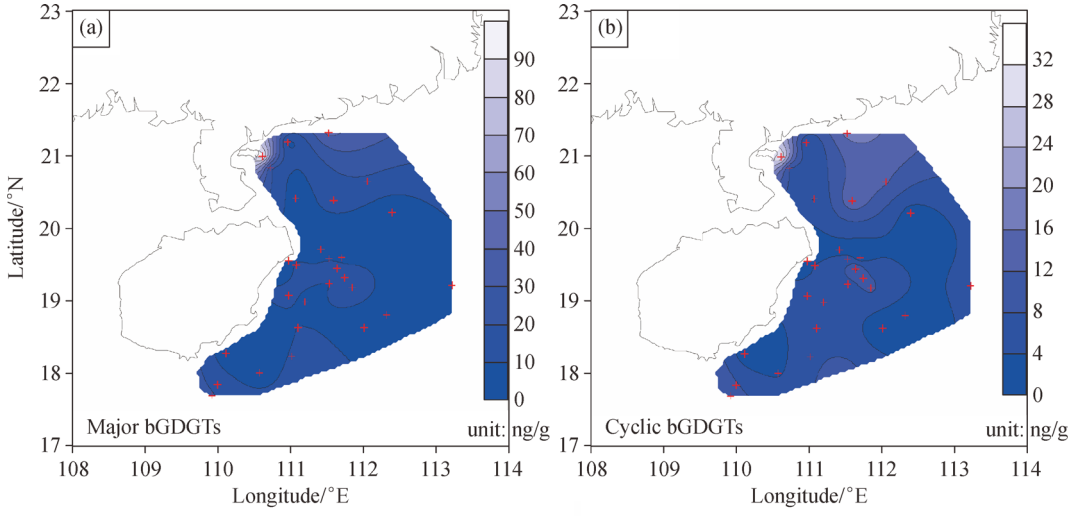

Fig. 4 The spatial distribution of bGDGTs concentration. Major bGDGTs = bGDGT-I + bGDGT-II + bGDGT-III. Cyclic bGDGTs = bGDGT-Ib + bGDGT-Ic + bGDGT-IIb + bGDGT-IIc + bGDGT-IIIb + bGDGT-IIIc.

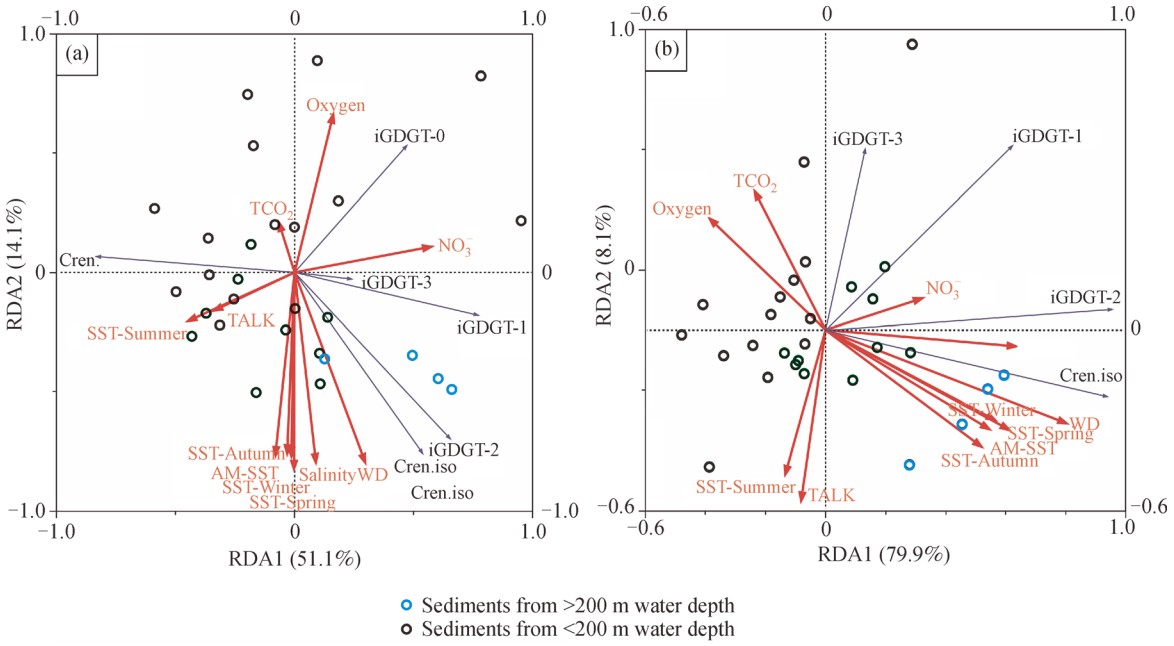

Fig. 6 Results of RDA analysis. (a) Triplot obtained by the RDA using six iGDGTs, 51.1% of the variation was explained by the first axis (RDA1) and 14.1% of the variation by the second axis (RDA2). (b) RDA triplot based on only four iGDGTs used for TEX_{86}^{H}. The RDA1 explained 79.9% of the variation and the RDA2 explained 8.1% of the variation. Blue open circles indicate the scores of the samples from > 200 m water depth and black open circles from < 200 m water depth.

Table 3 The RDA result with all iGDGT compounds applied

Variable	SST-Spring	NO_3^-	WD	Salinity	TALK	SST-Summer	TCO_2	SST-Autumn	AM-SST	SST-Winter	Oxygen
λ/%	12	17	12	9	8	3	3	1	1	0	0
p	0.006	0.024	0.028	0.044	0.108	0.25	0.284	0.538	0.548	0.788	0.936

Table 4 The RDA result with only four GDGT compounds applied

Variable	WD	NO_3^-	SST-Autumn	TCO_2	SST-Summer	TALK	AM-SST	SST-Winter	Salinity	Oxygen	SST-Spring
λ/%	52	8	7	8	7	2	2	2	1	0	0
p	0.002	0.002	0.008	0.012	0.044	0.044	0.108	0.152	0.156	0.648	0.978

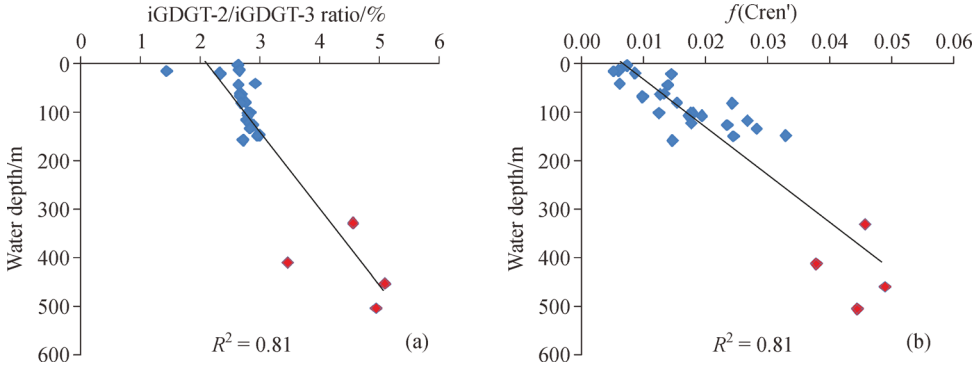

Fig. 7 Fractional abundance of crenarchaeol regio-isomer (Cren') and the iGDGT-2/iGDGT-3 ratio. The blue diamond represent the samples from < 200 m water depth and the red diamond from > 200 m water depth.

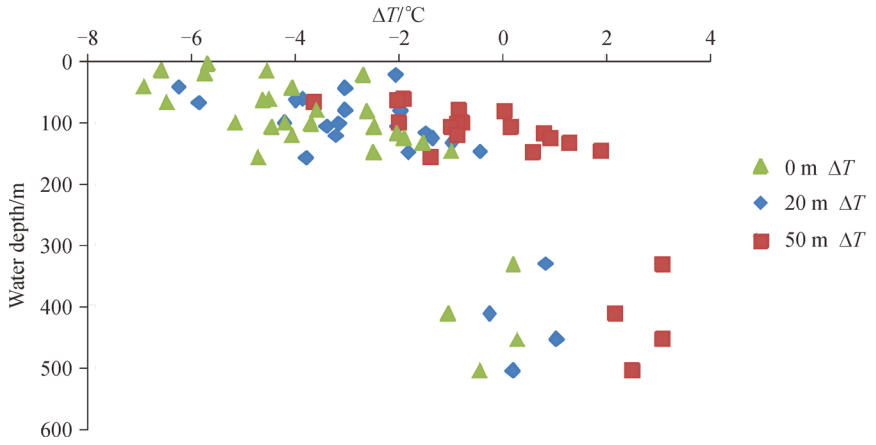

Fig. 8 Difference (ΔT) between TEX_{86}^{H} derived temperature and remote-sensing SSTs from different water depth. The green triangle represents annual mean sea surface temperature, the blue diamond represents the temperature in 20 m water depth and the red square represents the temperature in 50 m water depth.

(> 200 m) where the TEX_{86}^{H} derived temperature is close to the surface temperature (0−20 m) (Fig. 8).

The difference (ΔT) between TEX_{86}^{H}–derived temperature and seasonal remote-sensing SSTs is shown in Fig. 9. The temperature difference (ΔT) between TEX_{86}^{H} derived temperature and remote-sensing SSTs in summer and autumn is higher (up to 9°C) than that in annual mean SST. ΔT in spring and winter is in the range of ±6°C (−5.8°C −0.6°C, −2.8°C −3.4°C, respectively) (Fig. 9).

4 Discussion

The RDA results suggest that iGDGTs distribution is mainly influenced by water depth (WD), spring SST, nitrate, and salinity.

4.1 Influence of water depth

Water depth is the main controlling factor in the

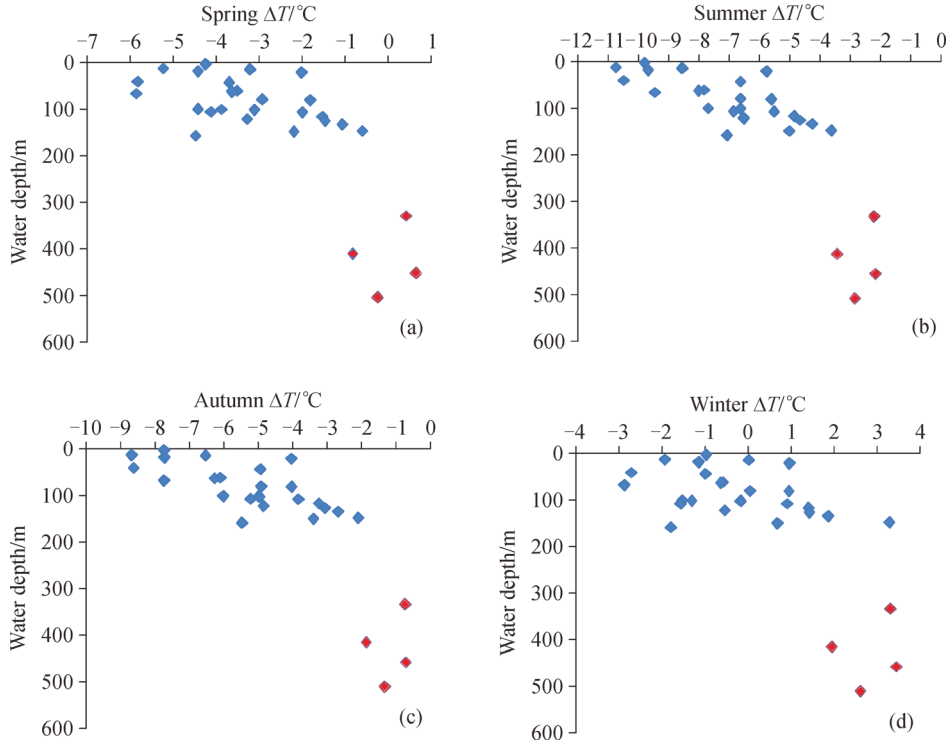

Fig. 9 Difference (ΔT) between TEX_{86}^{H}–derived temperature and seasonal remote-sensing SSTs. The blue diamond represents the samples from < 200 m water depth and the red diamond represents that from > 200 m water depth.

distribution of the four iGDGTs used in TEX_{86}^{H} ($\lambda = 52\%$, $p = 0.002$). The result is different from that observed in ECS where the distribution of iGDGTs is controlled by temperature (Lü et al., 2014). Such a discrepancy may be due to the different feedback of thaumarchaeota to environmental parameters in different regions (Turich et al., 2007). Recently, Hu et al. (2011) reported that the thaumarchaeota community in shallow water (< 200 m) is different from that in deep water (> 200 m) based on molecular biological analysis for the thaumarchaeotal sequence from the South China Sea. Water depth in eastern coastal seas of China (ECSC) is shallower than 150 m, suggesting that the thaumarchaeota in ECSC sediments may belong to similar communities.

Thaumarchaeota are primarily aerobic, ammonia-oxidizing chemoautotrophs. Because oxidation of ammonia may be a unifying metabolism for aerobic Thaumarchaeota (Pester et al., 2011), the abundance and activity of this group is commonly enumerated by counting amoA genes and mRNA transcripts as well as 16S rRNA genes. Various studies have shown that marine Thaumarchaeota fall into shallow- and deep-water phylogenetic clades (Francis et al., 2005; Hallam et al., 2006). Thaumarchaeotal sequences from the meso-bathypelagic (> 200 m water depth) waters are phylogenetically different from those retrieved from the epipelagic waters (0–200 m water depth) (Schouten et al., 2012; Villanueva et al., 2014). Environmental factors dictate the vertical distribution of these Archaea in the water column. Therefore, determining the depth in the water column in which the majority of archaeal GDGTs are produced is of paramount importance for researchers to understand the sources of these compounds in marine sediments.

The iGDGT-2/iGDGT-3 ratio also shows a significant correlation with water depth (Fig. 7(a)), suggesting that the archaea living in deep water is enriched in iGDGT-2 and the high iGDGT-2/iGDGT-3 ratio (> 3) may be used as a proxy for deep water archaea. This is similar to the results reported by Kim et al. (2015) in the global core top dataset that the fractional abundances of iGDGTs and water depth have strong correlations. However, in deeper waters, water depth (> 1000 m) is a better discriminator of iGDGT-2/iGDGT-3 ratios than SST in the modern dataset (Taylor et al., 2013). Wang et al. (2015) reported that the higher relative abundance of iGDGT-2 and iGDGT-3 between the Pearl River estuary and the coastal SCS (10−200 m) may be due to the non-thaumarchaeotal species, such as Marine Group II Euryarchaeota. The difference may be due to the different archaeal community in the Pearl River Estuary compared to the SCS with water depth > 200 m. In addition to the iGDGT-2/iGDGT-3 ratio, the fractional abundance of Crenarchaeol regio-isomer strongly increases with water depth (Fig. 7(b)), indicating that the crenarchaeol regio-isomer may be enriched in the deep thaumarchaeota or that it may be produced by crenarchaeota during diagenesis or both (Shah et al., 2008).

In addition, we found that the SST differences (ΔT) between TEX_{86}^{H} derived temperature and remote-sensing SST decreases with depth and the ΔT is lower than 1°C in the sediments with water depth > 200 m. Furthermore, the TEX_{86}^{H} derived temperature is close to the surface temperature (0−20 m) in the deep water sediment (> 200 m) (Fig. 8), suggesting that the TEX_{86}^{H} could be applied to trace the SST in the region with water depth > 200 m (Wucher and Schouten, 2005). This also implies that GDGTs from the deep water sediment may predominantly originate from surface water.

4.2 Influence of seasonal temperature

Temperature is the secondary factor to influence the distribution of iGDGTs, different from the results reported in the previous studies (Wei et al., 2011; Jia et al., 2012; Ge et al., 2013). If RDA is performed for six iGDGT compounds, spring SST plays a less important role on the iGDGTs distribution than WD ($p < 0.006$, $\lambda = 12\%$) (Table 3). However, if RDA is performed for only the four iGDGT compounds, the autumn SST and summer SST showed less influence than the WD (Table 4). The difference (ΔT) between TEX_{86}^{H} derived temperature and remote-sensing SSTs in summer and autumn is higher than those in the annual mean SST and ΔT in spring and winter, suggesting that TEX_{86}^{H} -derived SSTs are skewed towards spring/winter SSTs (Fig. 9). Moreover, it is noted that temperature is overestimated in colder (spring/winter) seasons with TEX_{86}^{H}. This is consistent with the fact that the seasonality of water temperature seems unlikely to be a major factor controlling the distribution of iGDGTs in the sediments of coastal SCS, as reported by Wang et al. (2015).

4.3 Influence of nutrients and salinity

Nutrient concentrations show impacts on the relative abundance of thaumarchaeota and thus affect GDGT concentrations and distributions. It is found that nitrate concentrations and the abundance of crenarchaeotal cells have a significant negative correlation (Murray et al., 1999). Our study shows that nitrate has a significant correlation with the relative abundance of individual iGDGT compounds in the RDA analyses ($p < 0.024$) (Table 3). This is similar to the result reported by Turich et al. (2007) that the mesopelagic zone/upwelling GDGTs showed a significant correlation with nitrate concentration. However, the correlation coefficient of the nitrate and TEX_{86}^{H} is low ($R = 0.1$, $p = 0.60$), indicating that the nitrate concentration may have a strong impact on the iGDGT concentrations, but not TEX_{86}^{H}. It may be due to that fact that nutrient and the other environmental factors could

jointly influence iGDGT distribution. Therefore, a partial RDA is performed to distinguish controlling factors. Obviously, nitrate can explain the largest contribution to variance (10.7%; Table 5), although the joint effect is 51%.

Table 5 Results of RDA and partial RDA showing variance (%) in iGDGT composition explained by all significant environment variables ($n = 28$)

Variable	Total		Unique	
	λ/%	p	λ/%	p
SST-Spring	12.0	0.006	4.0	0.722
NO_3^-	17.0	0.024	10.7	0.04
WD	12.0	0.028	0.6	0.654
Salinity	9.0	0.044	9.7	0.048
All variables	66.0			
Joint effects			51.0	

Some previous studies also reported that salinity may influence the abundance and community structure of Archaea associated with iGDGTs and archaeol (Turich and Freeman, 2011; Xie et al., 2014). Interestingly, the correlation between iGDGTs distribution and salinity is significant ($\lambda = 9\%$, $p = 0.044$) when six iGDGT compounds are considered in RDA, while the correlation is insignificant with only the four compounds. It suggests that salinity has a more significant influence on iGDGT-0 and Crenarchaeol than on the other iGDGT compounds. The low correlation coefficients are found between salinity and iGDGT-0 and crenarchaeol ($R^2 = 0.16$, 0.02, respectively). Wuchter et al. (2004) performed mesocosm studies with marine Crenarchaeota incubated at salinities of 27 ‰ and 35 ‰ to test the validity of the TEX_{86} proxy. Their results show that salinity does not substantially influence the GDGTs distribution in terms of TEX_{86} values. The reason remains unknown.

5 Conclusions

Concentration of total iGDGTs ranges from 15.03 to 534.18 ng/g, much higher than that of total bGDGTs (2.34−128.62 ng/g). Among the six iGDGT compounds, crenarchaeol and iGDGT-0 are the predominant compounds, which account for 65% and 20%, respectively. Concentrations of each iGDGT compound increase gradually eastward. RDA shows that water depth is the most significant factor to influence the iGDGTs distribution at the study region, different from that in ECS where temperature is the primary controlling factor . This may be due to the fact that thaumarchaeota communities are dependent on water depth. Furthermore, nitrate and salinity are found to show some influence on iGDGTs distribution. This study shows that theTEX_{86}^{H} may be considered as a robust proxy to trace the paleo-SST in the region with water depth > 200 m.

Acknowledgements We thank each member of the organic geochemistry group in the State Key Laboratory of Biogeology and Environmental Geology for technical support. We also thank Y. Qin, X. Chen and L. Gong from China University of Geosciences for help with data processing. We also thank Changbing Yang and Angelo R. Yang from The University of Texas in Austin for the language polishing. The research was funded by the National Natural Science Foundation of China (Grant No. 41376090), the ‘‘Strategic Priority Research Program’’ of the Chinese Academy of Sciences (XDA11020102), The Project of China Geological Survey (DD20160138), and Marine Safeguard Project (GZH201200503).

References

Basse A, Zhu C, Versteegh G J M, Fischer G, Hinrichs K, Mollenhauer G (2014). Distribution of intact and core tetraether lipids in water column profiles of suspended particulate matter off Cape Blanc, NW Africa. Org Geochem, 72: 1–13

De Rosa M, Esposito E, Gambacorta A, Nicolaus B, Bu'Lock J D (1980). Effects of temperature on ether lipid composition of Caldariella acidophila. Phytochemistry, 19(5): 827–831

Francis C A, Roberts K J, Beman J M, Santoro A E, Oakley B B (2005). Ubiquity and diversity of ammonia oxidizing archaea in water columns and sediments of the ocean. Proc Natl Acad Sci USA, 102 (41): 14683–14688

Ge H, Zhang C, Dang H, Zhu C, Jia G (2013). Distribution of tetraether lipids in surface sediments of the northern South China Sea: implications for TEX86 proxies. Geoscience Frontiers, 4(2): 223–229

Gliozzi A, Paoli G , De Rosa M , Gambacorta A (1983). Effect of isoprenoid cyclization on the transition temperature of lipids in thermophilic archaebacteria. Biochimica et Biophysica Acta (BBA) - Biomembranes, 735(2): 234–242

Hallam S J, Konstantinidis K T, Putnam N, Schleper C, Watanabe Y, Sugahara J, Preston C, de la Torre J, Richardson P M, DeLong E F (2006). Genomic analysis of the uncultivated marine crenarchaeote *Cenarchaeum symbiosum*. Proc Natl Acad Sci USA, 103(48): 18296–18301

Herndl G J, Reinthaler T, Teira E, van Aken H, Veth C, Pernthaler A, Pernthaler J (2005). Contribution of Archaea to total prokaryotic production in the deep Atlantic Ocean. Appl Environ Microbiol, 71 (5): 2303–2309

Hopmans E C, Weijers J W H, Schefuß E, Herfort L, Sinninghe Damsté J S, Schouten S (2004). A novel proxy for terrestrial organic matter in sediments based on branched and isoprenoid tetraether lipids. Earth Planet Sci Lett, 224(1−2): 107–116

Hu A, Jiao N, Zhang C (2011). Community structure and function of planktonic Crenarchaeota: changes with depth in the South China Sea. Microb Ecol, 62(3): 549–563

Hu J, Kawamura H, Hong H S, Qi Y (2000). Review on the currents in the South China Sea seasonal circulation South China Sea warm current and Kuroshio Intrusion. J Oceanogr, 56(6): 607–624

Huguet C, Hopmans E C, Febo-Ayala W, Thompson D H, Sinninghe Damste' J S, Schouten S (2006). An improved method to determine

the absolute abundance of glycerol dibiphytanyl glycerol tetraether lipids. Org Geochem, 37(9): 1036–1041

Jia G, Zhang J, Chen J, Peng P, Zhang C (2012). Archaeal tetraether lipids record subsurface water temperature in the South China Sea. Org Geochem, 50: 68–77

Karner M B, DeLong E F, Karl D M (2001). Archaeal dominance in the mesopelagic zone of the Pacific Ocean. Nature, 409(6819): 507–510

Kim J H, Schouten S, Rodrigo-Gámiz M, Rampen S, Marino G, Huguet C, Helmke P, Buscai R, Hopmans E, Pross J, Sangiorgi F, Middelburg J B M, Sinninghe Damsté J S (2015). Influence of deep-water derived isoprenoid tetraether lipids on the paleothermometer in the Mediterranean Sea. Geochim Cosmochim Acta, 150: 125–141

Kim J H, van der Meer J, Schouten S, Helmke P, Willmott V, Sangiorgi FKoç N, Hopmans E C, Damsté J S S (2010). New indices and calibrations derived from the distribution of crenarchaeal isoprenoid tetraether lipids: implications for past sea surface temperature reconstructions. Geochim Cosmochim Acta, 74(16): 4639–4654

Li F Y (1988). Determination of recent sedimentation rates by ^{210}Pb method in the South China Sea. Mark Sci, 3: 64–66

Li F Y, Yuan W (1991). Profile model of ^{210}Pb in the South China Sea, South Huanghai Sea and Bohai Sea. Mar Geol & Quaternary Geol, 11 (3): 35–43 (in Chinese)

Liu K K, Chao S Y, Shaw P T, Gong G C, Chen C C, Tang T Y (2002). Monsoon-forces chlorophyll distribution and primary production in the South China Sea: observations and a numerical study. Deep Sea Res Part I Oceanogr Res Pap, 49(8): 1387–1412

Lü X, Yang H, Song J, Versteegh G J M, Li X, Yuan H, Li N, Yang Y, Ding W, Xie S (2014). Sources and distribution of isoprenoid glycerol dialkyl glycerol tetraethers (GDGTs) in sediments from the east coastal sea of China: application of GDGT-based paleothermometry to a shallow marginal sea. Org Geochem, 75: 24–35

Murray A E, Blakis A, Massana R, Strawzewski S, Passow U, Alldredge A, Delong E F (1999). A time series assessment of planktonic archaealvariability in the Santa Barbara Channel. Aquat Microb Ecol, 20: 129–145

Ose T, Song Y K, Kitoh A (1997). Sea surface temperature in the South China Sea—An index for the Asian monsoon and ENSO system. J Meteorol Soc Jpn, 75: 1091–1107

Pernthaler A, Preston C M, Pernthaler J, DeLong E F, Amann R (2002). Comparison of fluorescently labeled oligonucleotide and polynucleotide probes for the detection of pelagic marine bacteria and archaea. Appl Environ Microbiol, 68(2): 661–667

Pester M, Schleper C, Wagner M (2011). The Thaumarchaeota: an emerging view of their phylogeny and ecophysiology. Curr Opin Microbiol, 14(3): 300–306

Peterse F, Kim J H, Schouten S, Kristensen D K, Koc N, Sinninghe Damsté J S (2009). Constraints on the application of the MBT/CBT palaeothermometer at high latitude environments (Svalbard, Norway). Organic Geochemistry, 40: 692–699

Powers L, Werne J P, Vanderwoude A J, Sinninghe Damsté J S, Hopmans E C, Schouten S (2010). Applicability and calibration of the TEX_{86} paleothermometer in lakes. Org Geochem, 41(4): 404–413

Qu T D (2001). Role of ocean dynamics in determining the mean seasonal cycle of the South China Sea surface temperature. J Geophys Res, 106(C4): 6943–6955

Schouten S, Hopmans E C, Schefuß E, Sinninghe Damste J S (2002). Distributional variations in marine crenarchaeotal membrane lipids: a new tool for reconstructing ancient sea water temperatures? Earth Planet Sci Lett, 204(1): 265–274

Schouten S, Huguet C, Hopmans E C, Kienhuis M M, Sinninghe Damste J S (2007). Analytical methodology for TEX_{86} paleothermometry by high-performance liquid chromatography/atmospheric pressure chemical ionization-mass spectrometry. Anal Chem, 79(7): 2940–2944

Schouten S, Pitcher A, Hopmans E C, Villanueva L, van Bleijswijk J, Sinninghe Damsté J S (2012). Intact polar and core glycerol dibiphytanyl glycerol tetraether lipids in the Arabian Sea oxygen minimum zone: I. Selective preservation and degradation in the water column and consequences for the TEX_{86}. Geochim Cosmochim Acta, 98: 228–243

Shah S R, Mollenhauer G, Ohkouchi N, Eglinton T I, Pearson A (2008). Origins of archaeal tetraether lipids in sediments: insights from radiocarbon analysis. Geochim Cosmochim Acta, 72(18): 4577–4594

Shen S, Lau M K (1995). Biennial oscillation associated with the East Asian summer monsoon and tropical sea surface temperatures. J Meteorol Soc Jpn, 73(1): 105–124

Shintani T, Yamamoto M, Chen M T (2011). Paleoenvironmental changes in the northern South China Sea over the past 28,000 years: a study of TEX86-derived sea surface temperatures and terrestrial biomarkers. Journal of Asian Earth Science, 40(6): 1221–1229

Sinninghe Damsté JS, Ossebaar J, Abbas B, Schouten S, Verschuren D (2009). Fluxes and distribution of tetraether lipids in an equatorial African lake: constraints on the application of the TEX_{86} palaeothermometer and BIT index in lacustrine settings. Geochimica et Cosmochimica Acta 73: 4232–4249

Taylor K W R, Huber M, Hollis C J, Hernandez-Sanchez M T, Pancost R D (2013). Re-evaluating modern and Palaeogene GDGT distributions: implications for SST reconstructions. Global Planet Change, 108: 158–174

Turich C, Freeman K H (2011). Archaeal lipids record paleosalinity in hypersaline systems. Org Geochem, 42: 1147–1157

Turich C, Freeman K H, Bruns M A, Conte M, Jones A D, Wakeham S G (2007). Lipids of marine Archaea: patterns and provenance in the water-column and sediments. Geochim Cosmochim Acta, 71(13): 3272–3291

Villanueva L, Schouten S, Sinninghe Damste′ J S (2014). Depth-related distribution of a key gene of the tetraether lipid biosynthetic pathway in marine Thaumarchaeota. Environ Microbiol, 10(17): 3527–3539

Walsh E M, Ingalls A E, Keil R G (2008). Sources and transport of terrestrial organic matter in Vancouver Island fjords and the Vancouver – Washington Margin: a multiproxy approach using d13Corg, lignin phenols, and the ether lipid BIT index. Limnol Oceanogr, 53(3): 1054–1063

Wang J X, Wei Y L, Wang P, Hong Y H, Zhang C L (2015). Unusually low TEX_{86} values in the transitional zone between Pearl River estuary and coastal South China Sea: impact of changing archaeal community composition. Chem Geol, 402: 18–29

Weber Y, De Jonge C, Rijpstra W I C, Hopmans E C, Stadnitskaia A, Schubert C J, Lehmann M F, Sinninghe Damsté J S, Niemann H (2015). Identification and carbon isotope composition of a novel branched GDGT isomer in lake sediments: evidence for lacustrine

branched GDGT production. Geochim Cosmochim Acta, 154: 118–129

Wei Y, Wang J, Liu J, Dong L, Li L, Wang H, Wang P, Zhao M, Zhang C (2011). Spatial variations in Archaeal lipids of surface water and core-top sediments in the South China Sea and their implications for Paleoclimate studies. Appl Environ Microbiol, 77(21): 7479–7489

Weijers J W H, Schouten S, van den Donker J C, Hopmans E C, Sinninghe Damsté J S (2007). Environmental controls on bacterial tetraether membrane lipid distribution in soils. Geochim Cosmochim Ac, 71(3): 703–713

Wuchter C, Schouten S (2005). Temporal and spatial variation in tetraether membrane lipids of marine Crenarchaeota in particulate organic matter: implications for TEX_{86} paleothermometry. Paleoceanography, 20: PA3013

Wuchter C, Schouten S, Coolen M J L, Sinninghe Damsté J S (2004). Temperature dependent variation in the distribution of tetraether membrane lipids of marine Crenarchaeota: implications for TEX86 paleothermometry. Paleoceanography, 19, PA4028

Xie W, Zhang C L, Zhou X D, Wang P (2014). Salinity-dominated change in community structure and ecological function of Archaea from the lower Pearl River to coastal South China Sea. Appl Microbiol Biotechnol, 98(18): 7971–7982

Yang H, Pancost R D, Tang C, Ding W, Dang X, Xie S (2014). Distributions of isoprenoid and branched glycerol dialkanol diethers in Chinese surface soils and a loess–paleosol sequence: implications for the degradation of tetraether lipids. Org Geochem, 66: 70–79

Zell C, Kim J-H, Dorhout D, Baas M, Sinninghe Damsté J S (2015). Sources and distributions of branched tetraether lipids and crenarchaeol along the Portuguese continental margin: implications for the BIT index. Cont Shelf Res, 96: 34–44

Zhang C L, Wang J X, Wei Y L, Zhu C, Huang L Q, Dong H L (2012). Production of branched tetraether lipids in the lower Pearl River and estuary: effects of extraction methods and impact on bGDGT proxies. Front Microbiol, 2(274): 1–18

Zhou H, Hu J, Spiro B, Peng P, Tang J (2014). Glycerol dialkyl glycerol tetraethers in surficial coastal and open marine sediments around China: indicators of sea surface temperature and effects of their sources. Palaeogeogr Palaeoclimatol Palaeoecol, 395: 114–121